Nano Research
2023, 16(4): 5383–5390

ISSN 1998-0124 CN 11-5974/O4
https://doi.org/10.1007/s12274-022-4740-5

Research Article

Ratiometric fluorescence immunoassay of SARS-CoV-2 nucleocapsid protein via Si-FITC nanoprobe-based inner filter effect

Guobin Mao[1,§], Yang Yang[3,§], Shijie Cao[1,2,§], Silu Ye[1], Yifang Li[1], Wei Zhao[1], Hongwei An[2], Yingxia Liu[3] (✉), Junbiao Dai[1], and Yingxin Ma[1] (✉)

[1] *CAS Key Laboratory of Quantitative Engineering Biology, Guangdong Provincial Key Laboratory of Synthetic Genomics and Shenzhen Key Laboratory of Synthetic Genomics, Shenzhen Institute of Synthetic Biology, Shenzhen Institutes of Advanced Technology, Chinese Academy of Sciences, Shenzhen 518055, China*

[2] *Guangxi University of Chinese Medicine, Nanning 530001, China*

[3] *Shenzhen Key Laboratory of Pathogen and Immunity, National Clinical Research Center for infectious disease, State Key Discipline of Infectious Disease, Shenzhen Third People's Hospital, Second Hospital Affiliated to Southern University of Science and Technology, Shenzhen 518112, China*

[§] *Guobin Mao, Yang Yang, and Shijie Cao contributed equally to this work.*

Received: 22 April 2022 / **Revised:** 1 July 2022 / **Accepted:** 3 July 2022

ABSTRACT

The global pandemic caused by severe acute respiratory syndrome coronavirus 2 (SARS-CoV-2) virus has necessitated rapid, easy-to-use, and accurate diagnostic methods to monitor the virus infection. Herein, a ratiometric fluorescence enzyme-linked immunosorbent assay (ELISA) was developed using Si-fluorescein isothiocyanate nanoparticles (FITC NPs) for detecting SARS-CoV-2 nucleocapsid (N) protein. Si-FITC NPs were prepared by a one-pot hydrothermal method using 3-aminopropyl triethoxysilane (APTES)-FITC as the Si source. This method did not need post-modification and avoided the reduction in quantum yield and stability. The p-nitrophenyl (pNP) produced by the alkaline phosphatase (ALP)-mediated hydrolysis of p-nitrophenyl phosphate (pNPP) could quench Si fluorescence in Si-FITC NPs via the inner filter effect. In ELISA, an immunocomplex was formed by the recognition of capture antibody/N protein/reporter antibody. ALP-linked secondary antibody bound to the reporter antibody and induced pNPP hydrolysis to specifically quench Si fluorescence in Si-FITC NPs. The change in fluorescence intensity ratio could be used for detecting N protein, with a wide linearity range (0.01–10.0 and 50–300 ng/mL) and low detection limit (0.002 ng/mL). The concentration of spiked SARS-CoV-2 N protein could be determined accurately in human serum. Moreover, this proposed method can accurately distinguish coronavirus disease 2019 (COVID-19) and non-COVID-19 patient samples. Therefore, this simple, sensitive, and accurate method can be applied for the early diagnosis of SARS-CoV-2 virus infection.

KEYWORDS

Si-fluorescein isothiocyanate (FITC) nanoparticles, ratiometric fluorescent probe, severe acute respiratory syndrome coronavirus 2 (SARS-CoV-2), inner filter effect, enzyme-linked immunosorbent assay (ELISA)

1 Introduction

In the past two decades, the development of luminescent nanoparticles for biological applications has been a major research focus [1, 2]. Fluorescent silicon nanoparticles (Si NPs) have become popular in optical applications because of their high quantum yield [3, 4], excellent stability [5], and low/non-toxicity [6]. Si NPs have been mainly used in various biosensors. Han et al. developed an exosome probe based on Si NPs to distinguish between normal and metastatic sentinel lymph nodes [7]. However, single-emission biosensors are vulnerable to the environment, probe concentration, and instrument [8]. Ratiometric fluorescent probes were specifically developed to overcome these shortcomings. In these probes, one signal is used as the reference and the other reacts with the analyte [9, 10]. These ratiometric fluorescent probes can be prepared by electrostatic interaction [11], covalent coupling [12], or metal–ligand interaction [13]. The electrostatic interaction method is simple, but its reproducibility is poor due to weak binding forces. The covalent coupling method is stable, but the fluorescence properties of the probe interfere with the coupling process. The metal–ligand interaction method is simple and stable, and has little influence on the probe [13]. While it seems an ideal choice for the construction of ratiometric fluorescent probes, the method can only be used to prepare metal nanoparticles [14]. The amino groups on the surface of Si NPs facilitate conjugation with biological molecules, such as nucleic acids, enzymes, and antibodies. Rhodamine B 5-isothiocyanate was coupled with Si NPs to construct a ratiometric fluorescence probe for pH imaging in living cells [15]. However, this method would lead to the reduction of quantum yield and stability during the coupling process. A simple and effective

Address correspondence to Yingxia Liu, yingxialiu@hotmail.com; Yingxin Ma, yx.ma1@siat.ac.cn

method for the construction of ratiometric fluorescent probes based on Si NPs remains to be identified.

Inner filter effect (IFE) is a phenomenon in the field of spectrofluorometry that refers to the absorption light of excitation and/or emission light of fluorophores by absorbers [16]. IFE provides a simple approach to design fluorescence sensors and is widely used in the development of biosensors [17] because it does not require any interaction between fluorophores and quenchers or complex modification of probes [18]. IFE-based sensors are mostly based on single-channel fluorescence change and are vulnerable to various concentration-related or physiological factors [19]. Ratiometric fluorescence probes can overcome these problems, however, the fluorescence intensity of probes in two peaks both reduced due to the excitation absorbed by the absorber, which challenges the construction of an IFE-based ratiometric system. Li et al. developed a ratiometric fluorescent platform for the detection of phosphate ions through the IFE-based oxidation of o-phenylenediamine by Fe-Zr bi-metal-organic framework [20]. Most of these methods based on the IFE quenching of probes by generating new fluorophores, require sophisticated design and are limited by the choice of probe-absorber pairs. There is a need to develop ratiometric fluorescence probes that are suitable for direct application in IFE-based sensors.

Severe acute respiratory syndrome coronavirus 2 (SARS-CoV-2) is a fatal virus that led to coronavirus disease 2019 (COVID-19) and has caused millions of deaths [21]. Given the magnitude of the pandemic, it is of great significance to develop novel methods for detecting SARS-CoV-2 [22]. Current methods for the diagnosis of SARS-CoV-2 can be broadly divided into three categories: nucleic acid detection, antibody detection, and antigen detection. Real-time reverse transcription polymerase chain reaction (RT-PCR) has been used widely as gold standard for SARS-CoV-2 diagnosis [23]. However, false positive results of nucleic acid detection may occur due to different factors, such as patient sampling quality, viral load, and cross contamination of amplification products [24]. Methods based on antigen–antibody detection are easier to operate. Reliable serological tests can provide more evidence about SARS-CoV-2 infection, and SARS-CoV-2 specific IgG and IgM have been used as evidence for COVID-19 diagnosis [25]. However, it is noteworthy that IgM and IgG positivity rate is low in the first week after symptom onset, and the diagnosis cannot be made directly by serological testing. Antigen detection is a reliable and convenient method for the diagnosis of SARS-CoV-2.

In this study, a ratiometric fluorescence immunoassay was developed based on Si-fluorescein isothiocyanate (FITC) NPs for detecting SARS-CoV-2 nucleocapsid (N) protein. Si-FITC NPs were prepared by a one-pot hydrothermal method without post-modification and purification, which well protected the luminous efficiency and stability. Synchronous fluorescence analysis was used to construct the IFE-based ratiometric sensor. The spectrum was composed of fluorescence intensity and corresponding excitation/emission wavelength by synchronously scanning the wavelengths of excitation and emission monochromators [26]. Two obvious fluorescence peaks, one of Si at 381 nm and the other of FITC at 489 nm, were observed in the synchronous fluorescence spectra of Si-FITC NPs. Alkaline phosphatase (ALP) catalyzed the hydrolysis of p-nitrophenyl phosphate (pNPP) to p-nitrophenyl (pNP) [27]. The absorption spectrum of the hydrolysate overlapped well with the excitation spectrum of Si, specifically reducing its fluorescence. The change in the fluorescence intensity ratio of Si-FITC NPs was directly related to ALP activity. ALP, as a labeled enzyme in enzyme-linked immunosorbent assay (ELISA) [28], mediated the detection of SARS-CoV-2 N protein. The detection of N protein exhibited a linearity range of 0.01–10.0 and 50–300 ng/mL, and the detection limit was 0.002 ng/mL. The concentration of N protein spiked in human serum could also be determined accurately. Therefore, the novel ELISA method with good sensitivity, selectivity, and accuracy proposed in this study could be applied clinically for the diagnosis of SARS-CoV-2 virus infection.

2 Experimental

2.1 Chemicals and materials

FITC isomer, sodium citrate tribasicdihydrate, 3-aminopropyl triethoxysilane (APTES), dimethyl sulfoxide (DMSO), trizma hydrochloride (Tris-HCl), glutamic acid, threonine, serine, proline, tyrosine, $CaCl_2$, KCl, $Zn(Ac)_2$, and $MgCl_2$ were purchased from Sigma. $FeSO_4$ and $MnSO_4$ were purchased from Sinopharm Chemical Reagent Co., Ltd. NH_4Cl was provided by Xilong Chemical Co., Ltd. $CuCl_2$ was purchased from Alfa Aesar. $FeCl_3$ was purchased from ACROS Organics. SARS-CoV-2 nucleocapsid-His recombinant protein, mouse anti-SARS-CoV-2 nucleocapsid mAb, rabbit anti-SARS-CoV-2 nucleocapsid mAb, and SARS-CoV-2 N protein ELISA kit were purchased from Sino Biological. Biotinylated goat anti-rabbit antibody was provided by Beyotime Biotechnology. Alkaline phosphatase was purchased from New England Biolabs. Alkaline phosphatase-conjugated streptavidin (SA-ALP) was provided by Beijing Bioss Biotechnology Co., Ltd. Disodium pNPP was provided by Shanghai Aladdin Biochemical Technology Co., Ltd.

2.2 Instruments and characterization

Time-resolved fluorescence spectra were recorded by the Edinburgh FLS1000 (Edinburgh Instruments). Fourier transform infrared (FT-IR) spectra were performed on the IRAffinity-1s spectrometer (Shimadzu). X-ray photoelectron spectroscopy (XPS) was obtained on the K-Alpha spectrometer (Thermo Scientific). Synchronous fluorescence spectra were tested using the F-7100 FL spectrophotometer. X-ray diffraction (XRD) spectra were obtained on the Ultima IV XRD system (Rigaku). Ultraviolet–visible (UV–vis) absorption spectra were recorded by Agilent (Cary 3500). Transmission electron microscopy (TEM) images were recorded by the JEM 2100 microscope (JEOL Ltd.).

2.3 Synthesis of Si-FITC NPs

APTES-FITC was obtained by dissolving 0.404 g FITC in 5 mL ethanol in a flask and adding 0.2 mL APTES into the above flask to react with FITC under dark and oxygen-free conditions for 20 h. Si-FITC NPs were prepared by a one-pot hydrothermal method, in which 0.184 g trisodium citrate was dissolved in 4 mL deionized water, and 1 mL APTES and 0.1 mL APTES-FITC were added to the above solution. The reaction solution was stirred for 10 min, transferred to a Teflon-lined stainless-steel autoclave, and reacted at 200 °C for 2 h. After that, the reaction product was purified with acetonitrile. The reaction product was mixed with acetonitrile in a volume ratio of 1:4 and centrifuged at 8,000 rpm for 15 min. The centrifugation and washing step were repeated twice, and the product thus obtained was vacuum-dried overnight at 60 °C to obtain Si-FITC NPs as crystals.

2.4 ALP-responsive fluorescence analysis

Different concentrations of ALP were added into Tris buffer (20 mM, pH 9.5) containing pNPP (300 μM) and Si-FITC NPs (1 mg/mL). The reaction solution was incubated at 37 °C for 30 min, and the synchronous fluorescence spectra were recorded.

2.5 Detection of N protein based on ALP-mediated ELISA

For the ALP-mediated ELISA system, capture antibody (100 μL, 1:1000) was added to a 96-well microplate and incubated with coating buffer (50 mM carbonate buffer, pH 9.6) at 4 °C overnight. After removing the coating buffer, the microplate was blocked with skimmed milk (300 μL, 2.5% w/t) at 37 °C for 2 h. Next, N protein, rabbit monoclonal antibody (100 μL, 1:5,000), biotinylated goat anti-rabbit secondary antibody (100 μL, 1:2,000), and SA-ALP (100 μL, 1:5,000) were incubated at 37 °C for 1 h, respectively, to form an immunocomplex. Then, 200 μL Tris-HCl buffer containing 500 μM pNPP was added and incubated at 37 °C for 1 h. The reaction solution was transferred to a centrifuge tube containing Si-FITC NPs (1 mg/mL), and the synchronous fluorescence spectra were recorded. The washing buffer (pH 7.4) contained 10 μM phosphate buffered solution (PBS)/0.05% Tween 20. The detection of N protein using commercial SARS-CoV-2 N protein ELISA kit was conducted as a control for sensitivity comparison.

2.6 Analysis of real samples

All clinical samples were collected from COVID-19 and non-COVID-19 patients hospitalized in Shenzhen Third People's Hospital, and confirmed by quantitative real-time PCR kit. The samples were inactivated by heating at 56 °C for 30 min and stored at −80 °C until further use. For detection, the samples (9 positives and 5 negatives) were lysed with sample lysis collection for 15 min, and diluted with PBS with a total volume of 200 μL. The samples were detected using this proposed method according to Section 2.5. All experimental waste was sterilized after detection.

3 Results and discussion

3.1 Characterization of as-prepared Si-FITC NPs

APTES-FITC was obtained by the reaction of FITC with APTES and used as the Si source to prepare Si-FITC NPs through a one-pot hydrothermal method (Scheme 1(a)). The UV–vis absorption spectra of the prepared Si-FITC NPs had two absorption peaks at 240 and 488 nm (Fig. 1(a)), which were the characteristic absorption peaks of FITC. The absorption peak at 260 nm was similar to that of free Si NPs. In the synchronous fluorescence spectrum, the two emission peaks of Si and FITC were located at 381 and 489 nm, respectively (Fig. 1(a)). Transmission electron microscopy images of the microstructure of Si-FITC NPs showed that Si-FITC NPs were globular and uniform particles with an obvious crystal structure (Fig. 1(b)). The size distribution ranged from 1.2 to 2.4 nm (Fig. 1(c)). FT-IR spectroscopy was collected to analyze the amino and hydroxyl groups on the surface of Si-FITC NPs. A characteristic absorption band at 1,027 cm^{-1} attributing to the stretching vibrations of Si–O and two shifts in the absorption peaks attributing to the stretching vibration of O–H (2,932 cm^{-1}) and N–H (3,361 cm^{-1}) were noted (Fig. S1 in the Electronic Supplementary Material (ESM)). The XRD spectrum showed a sharp characteristic diffraction peak at 23 degrees, suggesting that Si-FITC NPs were crystalline (Fig. S2 in the ESM). This peak did not significantly differ from the diffraction peak of Si NPs, and FITC did not affect the crystal structure of the NPs. The chemical structure and composition of Si-FITC NPs were analyzed by XPS. Si-FITC NPs were composed of Si, S, C, N, and O elements, located at 101.71, 172.58, 284.15, 398.66, and 530.88 eV, respectively (Fig. 1(d)). XPS of Si dots was implemented as

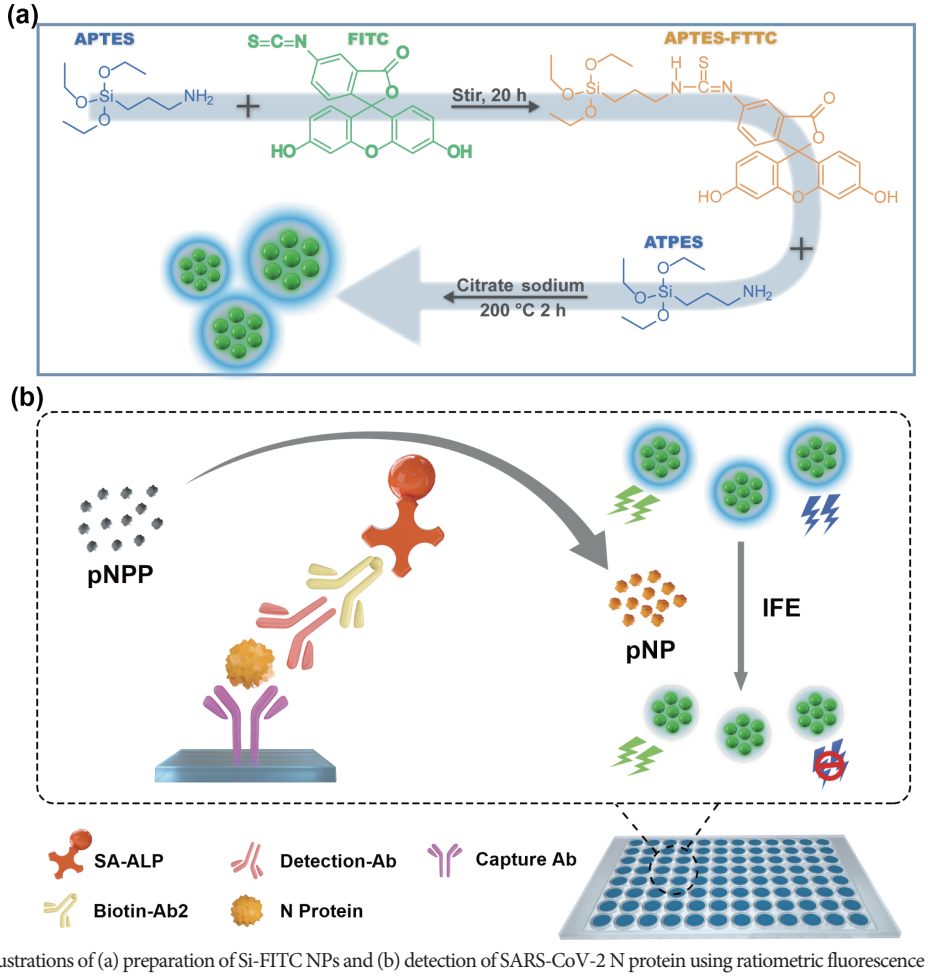

Scheme 1 Schematic illustrations of (a) preparation of Si-FITC NPs and (b) detection of SARS-CoV-2 N protein using ratiometric fluorescence ELISA.

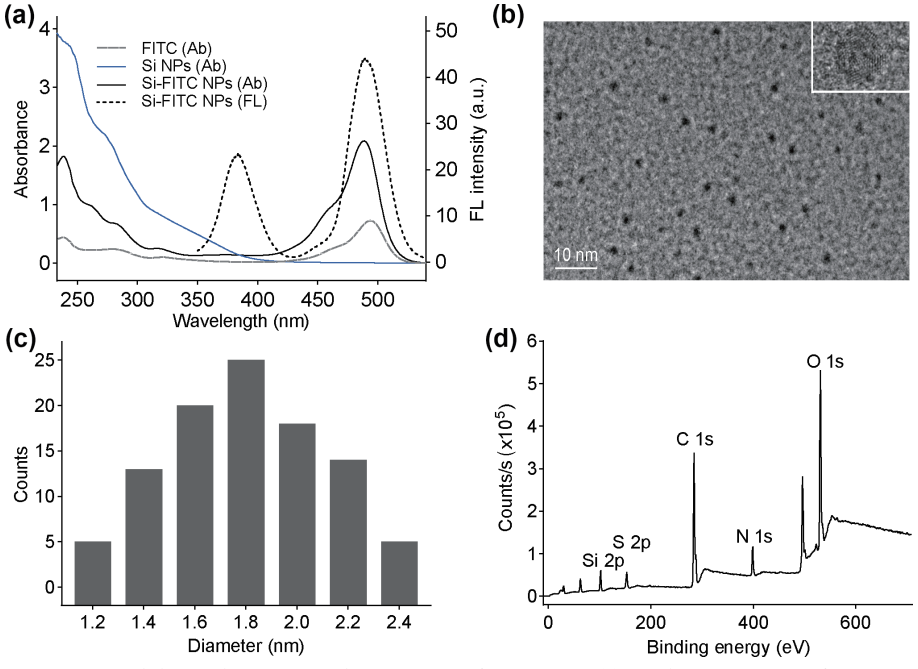

Figure 1 Optical properties, structure, and elemental composition characterization of Si-FITC NPs. (a) UV absorption spectra of FITC, Si NPs, and Si-FITC NPs and synchronous fluorescence spectrum of Si-FITC NPs. FITC, 10 μg/mL; Si NPs, 10 mg/mL; and Si-FITC NPs, 1 mg/mL. (b) Transmission electron microscopy image of Si-FITC NPs, inset: high resolution-transmission electron microscopy image. (c) A histogram of the size distribution of Si-FITC NPs. (d) XPS spectrum of Si-FITC NPs.

control. The functional composition of N and O in Si dots and Si-FITC NPs was listed in Table S1 in the ESM, which was different, indicating the conjugation of FITC with Si dots. In addition, FT-IR of FITC and Si-FITC NPs was investigated. The absorption peak at 2,031 cm^{-1} (probably attributing to –SCN) [29, 30] disappeared after the synthesis of Si-FITC NPs, which further indicated the conjugation of FITC with Si dots (Fig. S3 in the ESM).

3.2 Stability investigation of Si-FITC NPs

The photostability of Si-FITC NPs was evaluated by monitoring the fluorescence intensity under continuous radiation with a 350 V xenon lamp. The fluorescence intensity of Si dots in Si-FITC NPs decreased by about 20%, which was compared to that of individual Si dots. The intensity of FITC in Si-FITC NPs increased, and that of free FITC decreased by about 40% after irradiation (Fig. 2(a)). These results showed that both Si and FITC in Si-FITC NPs had better photostability due to the protection of Si coating. The blocking of FITC by Si coating improved the photostability of the ratiometric probe and allowed long-term imaging. The pH stability experiment was conducted in the pH range from 4 to 12. Free FITC was sensitive to pH, while Si-FITC NPs had a wide pH stability range, and the fluorescence did not significantly change under the different pH conditions (Fig. 2(b)

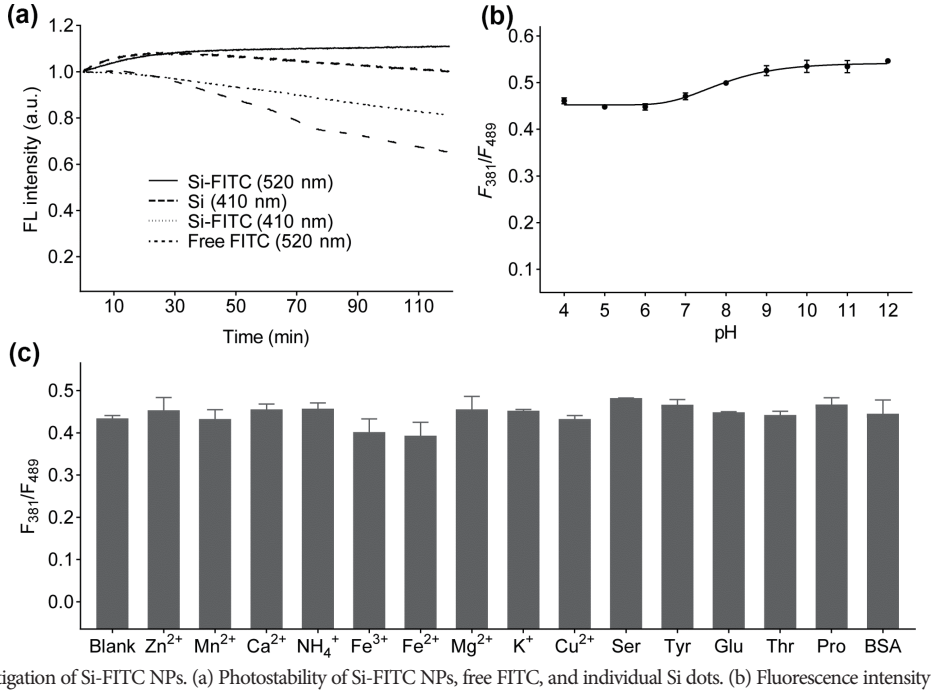

Figure 2 Stability investigation of Si-FITC NPs. (a) Photostability of Si-FITC NPs, free FITC, and individual Si dots. (b) Fluorescence intensity ratio of Si-FITC NPs in Tris buffer under different pH conditions. (c) Fluorescence intensity ratio response of Si-FITC NPs to different ions, amino acids, and biomacromolecule, whose concentration was 100 μM.

and Fig. S4 in the ESM). Therefore, FITC was predicted to be located inside Si-FITC NPs rather than on the surface of the NPs. The effects of some common ions, amino acids, and biomacromolecule in body fluids on the probe fluorescence were also studied (Fig. 2(c)). The addition of interfering substances (100 μM) had little effect on the fluorescence of Si-FITC NPs, indicating the remarkable anti-interference ability of Si-FITC NPs.

3.3 Analysis of ALP activity

ALP is an important hydrolase, generally distributed in mammalian body fluids and tissues. It can remove phosphate groups from biological molecules such as nucleic acids and proteins through dephosphorylation. In this study, pNP produced by the ALP-mediated hydrolysis of pNPP reduced the ratio of F_{381}/F_{489} by specifically quenching Si fluorescence without affecting FITC fluorescence in Si-FITC NPs (Fig. S5 in the ESM). The absorption peak of pNPP at 310 nm disappeared upon adding ALP, and a new absorption peak appeared at 400 nm, attributed to pNP. The absorption spectrum of pNP overlapped well with the excitation spectrum of Si, and pNP markedly quenched its fluorescence (Fig. 3(a)), indicating the IFE of pNP to Si dots. As shown in the UV–vis absorption spectrum, no significant difference was seen in the absorption peak of Si at 320 nm after adding pNPP and ALP (Fig. S6 in the ESM), indicating that the probe did not react with these components. The fluorescence decay curve of Si-FITC NPs was similar with or without ALP and pNPP (Fig. S7 in the ESM), indicating static fluorescence quenching as the main quenching mechanism. In the present system, pNPP slightly interfered with Si fluorescence, and the hydrolysate pNP specifically quenched the Si fluorescence by IFE. The difference in fluorescence intensity ratio ($\Delta(F_{381}/F_{489})$) before and after ALP addition was used for subsequent quantitative analysis. The reaction conditions were optimized to maximize ALP activity. When the concentration of pNPP was 300 μM (Fig. 3(b) and Fig. S8 in the ESM) and the pH value was 9.5 (Fig. 3(c) and Fig. S9 in the ESM), the change in fluorescence intensity ratio was the largest. Moreover, the reaction was completed within 30 min (Fig. 3(d)). Under this optimized condition, Si fluorescence in SI-FITC NPs decreased with an increase in ALP concentration (Fig. 3(e)). $\Delta(F_{381}/F_{489})$ correlated well with the ALP concentration from 0.5 to 20.0 U/L (Fig. 3(f)). The detection limit was 0.08 U/L, lower than most previously reported values (Table S2 in the ESM).

3.4 ALP-mediated ratiometric fluorescence ELISA for N protein detection

Millions of people have died due to COVID-19 [31], making diagnostic tests extremely critical for the rapid and accurate confirmation of virus infection [32]. Compared with nucleic acid or antibody-based detection methods, the antigen assay method for the diagnosis of SARS-CoV-2 infection displays the advantages of simple operation, high speed, and high accuracy [33]. SARS-CoV-2 N protein plays an important role in the transcription,

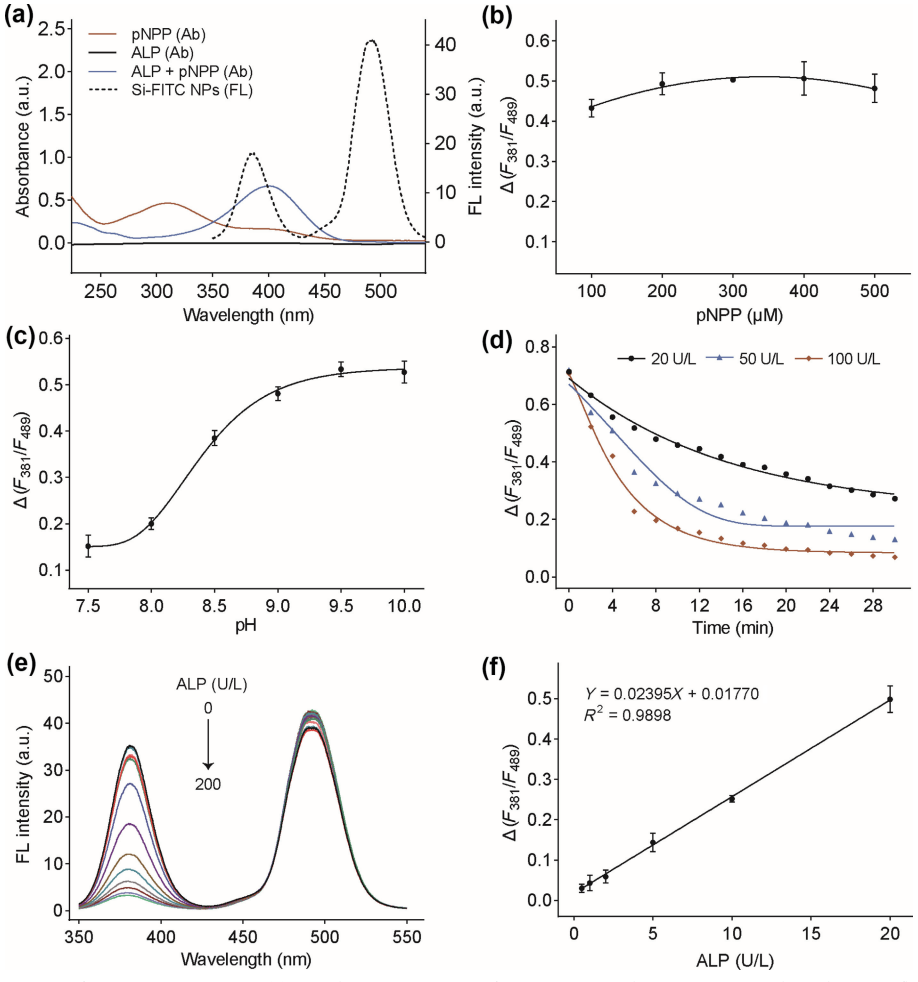

Figure 3 Fluorescence response of Si-FITC NPs to ALP. (a) UV absorption spectra of ALP, pNPP, and ALP + pNPP and synchronous fluorescence spectrum of Si FITC NPs. (b) Change in the fluorescence intensity ratio of Si-FITC NPs upon the addition of different concentrations of pNPP and 20 U/L ALP. (c) Change in the fluorescence intensity ratio of Si-FITC NPs upon the addition of 300 μM pNPP and 20 U/L ALP under different pH conditions. (d) Optimization of reaction times for ALP detection. The concentrations of ALP were 20, 50, and 100 U/L. (e) Synchronous fluorescence spectra of the Si-FITC NPs in Tris buffer containing 300 μM pNPP in response to ALP with different concentration. (f) Calibration curve for ALP detection. $\Delta(F_{381}/F_{489}) = (F_{381}/F_{489})_0 - (F_{381}/F_{489})_x$, and x = 20 U/L ALP.

replication, and packaging of viral RNA, which is structurally more conservative than other proteins [34]. Therefore, N protein is used as the main target for the diagnosis of SARS-CoV-2 infection. ALP has been widely used as a labeling enzyme in ELISA. In this study, we proposed a highly selective and sensitive ALP-mediated immunoassay for the ratiometric fluorescence detection of N protein.

The immunocomplex consisted of ALP-linked secondary antibody, reporter antibody, and N protein, and the capture antibody was coated on a 96-well plate. pNPP was added to generate pNP, which specifically quenched the Si fluorescence in the probe by IFE. N protein could be detected by observing the change in $\Delta(F_{381}/F_{489})$. The sensitivity of the method was improved by optimizing the concentration and dilution of pNPP and SA-ALP, respectively. The best detection was possible when the pNPP concentration was 500 μM and the SA-ALP dilution was 1:5,000 (Figs. 4(a) and 4(b)). Under this condition, the increase in N protein concentration was accompanied by a corresponding quenching of Si fluorescence (Fig. 4(c)), and a good linear relationship was obtained between $\Delta(F_{381}/F_{489})$ and the logarithm of N protein concentration (0.01–10.0 and 50–300 ng/mL) (Figs. 4(d) and 4(e)). The detection limit was 0.002 ng/mL. The commercial SARS-CoV-2 N protein ELISA kit was used for N protein detection. As shown in Fig. S10 in the ESM, with the increase of N protein concentration, the absorption intensity enhanced, and the limit of detection was 0.037 ng/mL, which was higher than that of our method. This result indicated the high sensitivity of our method, which was higher than most previously reported methods including antibody and antigen detection (Table S3 in the ESM).

The specificity of an ELISA method depends on the target recognition of the antigen by the antibody. The selectivity of this method to other proteins, including bovine serum albumin (BSA) and SARS-CoV-2 S protein, was studied. BSA is widely present in human serum. There was little change upon the addition of BSA or SARS-CoV-2 S protein, even at 10 times the concentration of N protein (Fig. 4(f)). The results indicated that the developed ELISA system had great specificity for the N protein detection and no cross-reactivity with other proteins.

3.5 Detection of N protein in human serum

The feasibility of this method for detecting the concentration of SARS-CoV-2 N protein in human serum was next evaluated. Human serum was spiked with N protein with different concentrations (10.00 or 100.00 ng/mL), and the concentration was then calculated according to the linear relationship of N protein detection. The spiked sample recovery and relative standard deviation were in the range of 95.17%–107.41% and 5.44%–13.01%, respectively (Table S4 in the ESM). The results indicated that the ratiometric fluorescence ELISA can be applied for the rapid and precise detection of N protein in human serum.

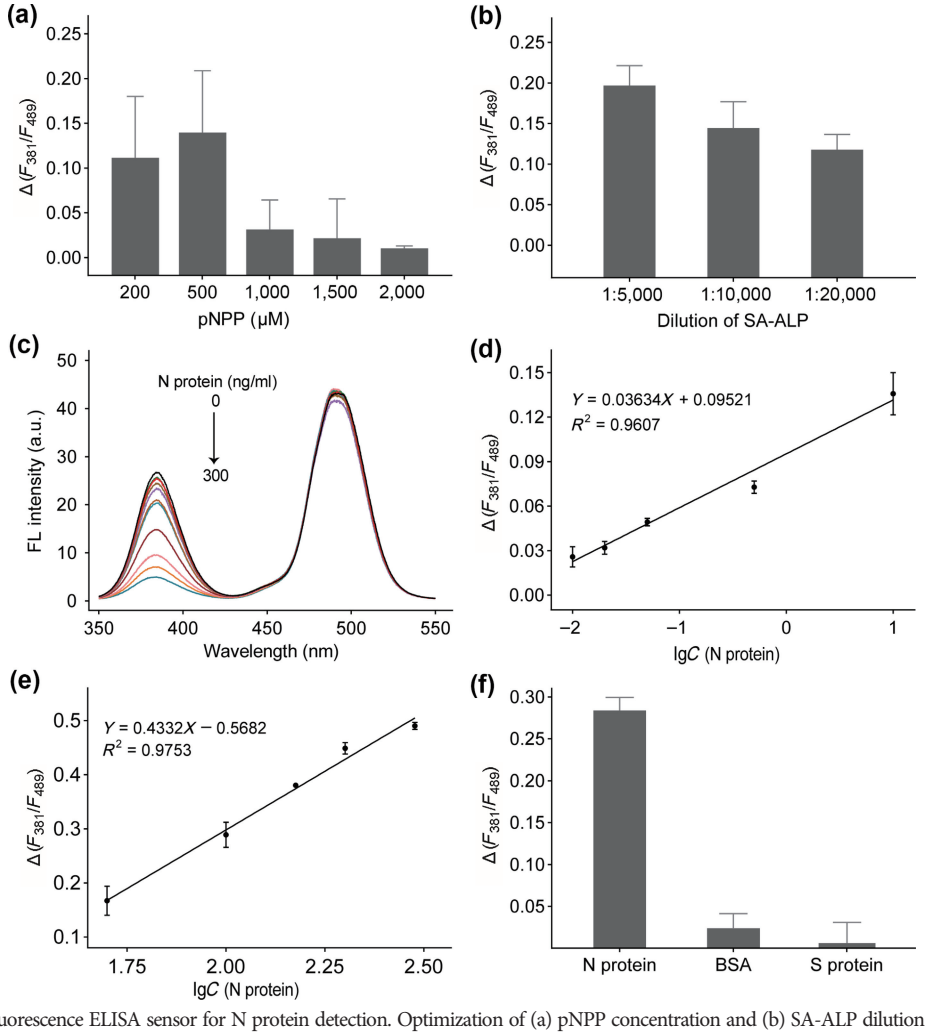

Figure 4 Ratiometric fluorescence ELISA sensor for N protein detection. Optimization of (a) pNPP concentration and (b) SA-ALP dilution for N protein detection. (c) Fluorescence spectra of Si-FITC NPs in response to different concentration of N protein. (d) and (e) Calibration curve for SARS-CoV-2 N protein detection. (f) Investigation of the selectivity of SARS-CoV-2 N protein detection against other interfering proteins; the concentration of N protein was 100 ng/mL, and the concentration of other interfering proteins was 1,000 ng/mL.

3.6 Validation with clinical samples

To evaluate the utility of our proposed method for the detection of N protein in clinical samples, oropharyngeal or nasopharyngeal swabs from the COVID-19 and non-COVID-19 patients were collected. The positive and negative were determined by quantitative real-time PCR, which were further evaluated using our proposed method. As shown in Fig. 5, the change of fluorescence intensity ratio was much larger than that of the normal healthy samples, which the fluorescence intensity ratio change was very low. The detection limit was 0.064 ng/mL. The fluorescence intensity ratio change of the positive was higher than LOD, and that of the negative was lower than LOD, which was mean +3 times of relative standard deviation (RSD). In addition, the fluorescence intensity ratio change was negatively corrected with CT value (listed in Table S5 in the ESM), indicating the good accuracy of this method. Based on these preliminary results, this proposed ratiometric ELISA method is capable to distinguish samples from COVID-19 and non-COVID-19 patients efficiently. This method has potential for clinical diagnosis in the laboratory or hospital, however, the reproducibility and stability need to be further improved.

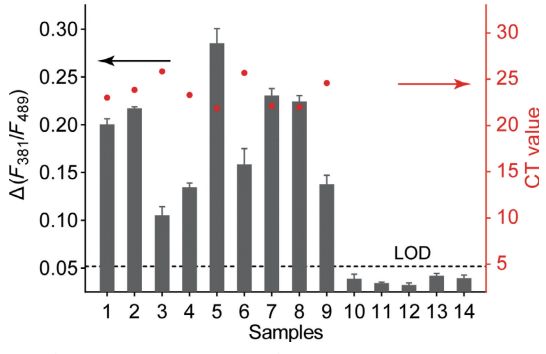

Figure 5 Fluorescence intensity ratio change in response to COVID-19 (1–9) and non-COVID-19 (10–14) patient samples, and LOD equals to mean +3 times of RSD.

4 Conclusions

In summary, we constructed a ratiometric fluorescence probe, Si-FITC NPs, for immunoassay of SARS-CoV-2 N protein. Si-FITC NPs were prepared by a one-pot hydrothermal method without post-modification and purification, which well protected the luminous efficiency and stability. The pNP produced by the ALP-mediated hydrolysis of pNPP could quench Si fluorescence in Si-FITC NPs via the inner filter effect. ALP-mediated hydrolysate quenched Si fluorescence in Si-FITC NPs without affecting FITC fluorescence, providing a simple and universal method for N protein detection. The method had excellent sensitivity and selectivity, and the detection limit was 0.002 ng/mL, which was better than that by the commercial ELISA kit. The ratiometric fluorescence ELISA can be used for the N protein detection in human serum with recovery rate of 95.17%–107.41%. Then, the COVID-19 patients and the non-COVID-19 individuals were distinguishable by this proposed ratiometric ELISA method. In addition, this method not only improved the detection sensitivity of ELISA, but also broadened the application of IFE-based ratiometric sensors.

Acknowledgements

This work was supported by the National Key Research and Development Program of China (No. 2021YFA0910900), the National Natural Science Foundation (No. 22104147), Youth Innovation Promotion Association CAS (No. 2021359), the Natural Science Foundation of Guangdong (Nos. 2018B030306046 and 2020A1515111130), Guangdong Provincial Key Laboratory of Synthetic Genomics (No. 2019B030301006), Shenzhen Science and Technology Program (No. KQTD20180413181837372), and Shenzhen Outstanding Talents Training Fund.

Electronic Supplementary Material: Supplementary material (characterization of Si-FITC NPs (FTIR spectrum, XRD spectra, and synchronous fluorescence spectra); condition optimization of ALP response (fluorescence intensity ratio change); mechanism investigation of ALP response (fluorescence lifetime decay curves and UV–vis absorption spectra); detection of N protein using commercial ELISA Kit; analytical performance of assays for ALP detection or SARS-CoV-2 N protein detection; and determination results of SARS-CoV-2 N protein in human serum) is available in the online version of this article at https://doi.org/10.1007/s12274-022-4740-5.

References

[1] Ma, Y. X.; Mao, G. B.; Huang, W. R.; Wu, G. Q.; Yin, W.; Ji, X. H.; Deng, Z. S.; Cai, Z. M.; Zhang, X. E.; He, Z. K. et al. Quantum dot nanobeacons for single RNA labeling and imaging. *J. Am. Chem. Soc.* **2019**, *141*, 13454–13458.

[2] Devi, P.; Saini, S.; Kim, K. H. The advanced role of carbon quantum dots in nanomedical applications. *Biosens. Bioelectron.* **2019**, *141*, 111158.

[3] Zhong, Y. L.; Peng, F.; Bao, F.; Wang, S. Y.; Ji, X. Y.; Yang, L.; Su, Y. Y.; Lee, S. T.; He, Y. Large-scale aqueous synthesis of fluorescent and biocompatible silicon nanoparticles and their use as highly photostable biological probes. *J. Am. Chem. Soc.* **2013**, *135*, 8350–8356.

[4] So, W. Y.; Li, Q.; Legaspi, C. M.; Redler, B.; Koe, K. M.; Jin, R. C.; Peteanu, L. A. Mechanism of ligand-controlled emission in silicon nanoparticles. *ACS Nano* **2018**, *12*, 7232–7238.

[5] Han, Y. X.; Chen, Y. L.; Liu, J. J.; Niu, X. Y.; Ma, Y. X.; Ma, S. D.; Chen, X. G. Room-temperature synthesis of yellow-emitting fluorescent silicon nanoparticles for sensitive and selective determination of crystal violet in fish tissues. *Sens. Actuators B:Chem.* **2018**, *263*, 508–516.

[6] Zhou, Y. F.; Zhang, Y.; Zhong, Y. L.; Fu, R.; Wu, S. C.; Wang, Q.; Wang, H. Y.; Su, Y. Y.; Zhang, H. M.; He, Y. The *in vivo* targeted molecular imaging of fluorescent silicon nanoparticles in *Caenorhabditis elegans*. *Nano Res.* **2018**, *11*, 2336–2346.

[7] Han, J. F.; Zhang, L.; Cui, M. Y.; Su, Y. Y.; He, Y. Rapid and accurate detection of lymph node metastases enabled through fluorescent silicon nanoparticles-based exosome probes. *Anal. Chem.* **2021**, *93*, 10122–10131.

[8] Jiao, Y.; Gao, Y. F.; Meng, Y. T.; Lu, W. J.; Liu, Y.; Han, H.; Shuang, S. M.; Li, L.; Dong, C. One-step synthesis of label-free ratiometric fluorescence carbon dots for the detection of silver ions and glutathione and cellular imaging applications. *ACS Appl. Mater. Interfaces* **2019**, *11*, 16822–16829.

[9] Park, S. H.; Kwon, N.; Lee, J. H.; Yoon, J.; Shin, I. Synthetic ratiometric fluorescent probes for detection of ions. *Chem. Soc. Rev.* **2020**, *49*, 143–179.

[10] Yue, Y. K.; Huo, F. J.; Ning, P.; Zhang, Y. B.; Chao, J. B.; Meng, X. M.; Yin, C. X. Dual-site fluorescent probe for visualizing the metabolism of Cys in living cells. *J. Am. Chem. Soc.* **2017**, *139*, 3181–3185.

[11] Lan, M. H.; Zhang, J. F.; Chui, Y. S.; Wang, P. F.; Chen, X. F.; Lee, C. S.; Kwong, H. L.; Zhang, W. J. Carbon nanoparticle-based ratiometric fluorescent sensor for detecting mercury ions in aqueous media and living cells. *ACS Appl. Mater. Interfaces* **2014**, *6*, 21270–21278.

[12] Zou, C. C.; Foda, M. F.; Tan, X. C.; Shao, K.; Wu, L.; Lu, Z. C.; Bahlol, H. S.; Han, H. Y. Carbon-dot and quantum-dot-coated dual-

emission core-satellite silica nanoparticles for ratiometric intracellular Cu^{2+} imaging. *Anal. Chem.* **2016**, *88*, 7395–7403.

[13] Mao, G. B.; Cai, Q.; Wang, F. B.; Luo, C. L.; Ji, X. H.; He, Z. K. One-step synthesis of Rox-DNA functionalized CdZnTeS quantum dots for the visual detection of hydrogen peroxide and blood glucose. *Anal. Chem.* **2017**, *89*, 11628–11635.

[14] Ma, J. W.; Chen, Y. G.; Chen, L.; Wang, L. Y. Ternary Pd-Ni-P nanoparticle-based nonenzymatic glucose sensor with greatly enhanced sensitivity achieved through active-site engineering. *Nano Res.* **2017**, *10*, 2712–2720.

[15] Chu, B. B.; Wang, H. Y.; Song, B.; Peng, F.; Su, Y. Y.; He, Y. Fluorescent and photostable silicon nanoparticles sensors for real-time and long-term intracellular pH measurement in live cells. *Anal. Chem.* **2016**, *88*, 9235–9242.

[16] Yan, X.; Li, H. X.; Han, X. S.; Su, X. G. A ratiometric fluorescent quantum dots based biosensor for organophosphorus pesticides detection by inner-filter effect. *Biosens. Bioelectron.* **2015**, *74*, 277–283.

[17] Li, H. Y.; Lin, H. Y.; Lv, W. X.; Gai, P. P.; Li, F. Equipment-free and visual detection of multiple biomarkers via an aggregation induced emission luminogen-based paper biosensor. *Biosens. Bioelectron.* **2020**, *165*, 112336.

[18] Zhang, J. Y.; Zhou, R. H.; Tang, D. D.; Hou, X. D.; Wu, P. Optically-active nanocrystals for inner filter effect-based fluorescence sensing: Achieving better spectral overlap. *TrAC Trends Anal. Chem.* **2019**, *110*, 183–190.

[19] Zhai, W. Y.; Wang, C. X.; Yu, P.; Wang, Y. X.; Mao, L. Q. Single-layer MnO_2 nanosheets suppressed fluorescence of 7-hydroxycoumarin: Mechanistic study and application for sensitive sensing of ascorbic acid *in vivo*. *Anal. Chem.* **2014**, *86*, 12206–12213.

[20] Li, X.; Liu, P.; Niu, X. H.; Ye, K.; Ni, L.; Du, D.; Pan, J. M.; Lin, Y. H. Tri-functional Fe-Zr bi-metal-organic frameworks enable high-performance phosphate ion ratiometric fluorescent detection. *Nanoscale* **2020**, *12*, 19383–19389.

[21] Zhu, N.; Zhang, D. Y.; Wang, W. L.; Li, X. W.; Yang, B.; Song, J. D.; Zhao, X.; Huang, B. Y.; Shi, W. F.; Lu, R. J. et al. A novel coronavirus from patients with pneumonia in China, 2019. *N. Engl. J. Med.* **2020**, *382*, 727–733.

[22] Ravi, N.; Cortade, D. L.; Ng, E.; Wang, S. X. Diagnostics for SARS-CoV-2 detection: A comprehensive review of the FDA-EUA COVID-19 testing landscape. *Biosens. Bioelectron.* **2020**, *165*, 112454.

[23] Wang, Y.; Yan, T. H.; Mei, K. N.; Rao, D. P.; Wu, W. J.; Chen, Y.; Peng, Y. P.; Wang, J. Y.; Wu, S. Q.; Zhang, Q. C. Nanomechanical assay for ultrasensitive and rapid detection of SARS-CoV-2 based on peptide nucleic acid. *Nano Res.*, in press, https://doi.org/10.1007/s12274-022-4333-3.

[24] Jang, A. S.; Kumar, P. P. P.; Lim, D. K. Attomolar sensitive magnetic microparticles and a surface-enhanced Raman scattering-based assay for detecting SARS-CoV-2 nucleic acid targets. *ACS Appl. Mater. Interfaces* **2022**, *14*, 138–149.

[25] Chen, M. R.; Cui, D. Z.; Zhao, Z. Y.; Kang, D.; Li, Z.; Albawardi, S.; Alsageer, S.; Alamri, F.; Alhazmi, A.; Amer, M. R. et al. Highly sensitive, scalable, and rapid SARS-CoV-2 biosensor based on In_2O_3 nanoribbon transistors and phosphatase. *Nano Res.* **2022**, *15*, 5510–5516.

[26] Mao, G. B.; Zhang, Q.; Yang, Y. L.; Ji, X. H.; He, Z. K. Facile synthesis of stable CdTe/CdS QDs using dithiol as surface ligand for alkaline phosphatase detection based on inner filter effect. *Anal. Chim. Acta* **2019**, *1047*, 208–213.

[27] Chen, W.; Habibul, N.; Liu, X. Y.; Sheng, G. P.; Yu, H. Q. FTIR and synchronous fluorescence heterospectral two-dimensional correlation analyses on the binding characteristics of copper onto dissolved organic matter. *Environ. Sci. Technol.* **2015**, *49*, 2052–2058.

[28] Zhao, D.; Li, J.; Peng, C. Y.; Zhu, S. Y.; Sun, J.; Yang, X. R. Fluorescence immunoassay based on the alkaline phosphatase triggered *in situ* fluorogenic reaction of o-phenylenediamine and ascorbic acid. *Anal. Chem.* **2019**, *91*, 2978–2984.

[29] Wei, Q. S.; Zhou, D. X.; Li, X. Q.; Chen, Y. W.; Bian, H. T. Structural dynamics of dimethyl sulfoxide aqueous solutions investigated by ultrafast infrared spectroscopy: Using thiocyanate anion as a local vibrational probe. *J. Phys. Chem. B* **2018**, *122*, 12131–12138.

[30] Vu, H. P.; Moreau, J. W. Thiocyanate adsorption on ferrihydrite and its fate during ferrihydrite transformation to hematite and goethite. *Chemosphere* **2015**, *119*, 987–993.

[31] Castro, M. C.; Gurzenda, S.; Turra, C. M.; Kim, S.; Andrasfay, T.; Goldman, N. Reduction in life expectancy in Brazil after COVID-19. *Nat. Med.* **2021**, *27*, 1629–1635.

[32] Yang, Y.; Yang, M. H.; Yuan, J.; Wang, F. X.; Wang, Z. Q.; Li, J. X.; Zhang, M. X.; Xing, L.; Wei, J. L.; Peng, L. et al. Laboratory diagnosis and monitoring the viral shedding of SARS-CoV-2 infection. *Innovation* **2020**, *1*, 100061.

[33] Dinnes, J.; Deeks, J. J.; Berhane, S.; Taylor, M.; Adriano, A.; Davenport, C.; Dittrich, S.; Emperador, D.; Takwoingi, Y.; Cunningham, J. et al. Rapid, point-of-care antigen and molecular-based tests for diagnosis of SARS-CoV-2 infection. *Cochrane Database Syst. Rev.* **2021**, *2021*, CD013705.

[34] Kang, S. S.; Yang, M.; Hong, Z. S.; Zhang, L. P.; Huang, Z. X.; Chen, X. X.; He, S. H.; Zhou, Z. L.; Zhou, Z. C.; Chen, Q. Y. et al. Crystal structure of SARS-CoV-2 nucleocapsid protein RNA binding domain reveals potential unique drug targeting sites. *Acta Pharm. Sin. B* **2020**, *10*, 1228–1238.